Mechanisms of atomic diffusion on the flat, stepped, and faceted surfaces of Al(110)

Yogesh Tiwary[1] and Kristen A. Fichthorn[1,2,*]

[1]*Department of Chemical Engineering, The Pennsylvania State University, University Park, Pennsylvania 16802, USA*

[2]*Department of Physics, The Pennsylvania State University, University Park, Pennsylvania 16802, USA*

(Received 15 December 2009; revised manuscript received 24 February 2010; published 14 May 2010)

Using first-principles calculations based on density-functional theory, we elucidate mechanisms and energy barriers for atomic diffusion on Al(110), Al(100), and Al(111), up and down (100) and (111) steps on Al(110), and between the (100), (111), and (110) facets of Al. We find that the energetically preferred mechanism for adatom diffusion on Al(110) is a diagonal exchange between the adatom and the substrate, which leads to isotropic diffusion on this anisotropic surface. Similarly, diagonal exchange involving three atoms is the preferred mechanism for atoms to ascend and descend the (100) and (111) steps. The descent of atoms over the (100) steps is hindered by diffusion to the step edge while for the (111) steps, it is hindered by diffusion over the edge. Energy barriers to ascend from (110) to (100) or (111) facets depend on facet height. Neighboring adatoms can significantly influence diffusion-energy barriers and simple approaches cannot predict this complex behavior. The energy barriers for dimers to climb from the (110) to the (100) and (111) facets are lower than those for isolated adatoms.

DOI: 10.1103/PhysRevB.81.195421 PACS number(s): 68.35.Fx, 68.35.Ja, 66.30.Fq, 68.55.A−

I. INTRODUCTION

Achieving the controlled self-assembly of nanostructures in thin-film epitaxy is an important goal that could enable applications in catalysis,[1,2] (opto)electronics,[3–8] quantum computing,[9] and magnetic data storage.[10] Although the growth of self-assembled structures has been observed experimentally in many heteroepitaxial systems, as well as in homoepitaxy, the ability to predict assembly from first principles is currently limited. Since thin-film growth often occurs away from equilibrium, kinetic phenomena govern morphological evolution and a predictive model must accurately include all the relevant kinetic processes. These include phenomena associated with deposition, such as downward funneling,[11] shadowing,[12] and steering,[13] as well as a multitude of different processes that govern surface diffusion. If all these important processes can be identified, they can be incorporated into a kinetic Monte-Carlo (KMC) simulation[14] that can predict the interfacial morphology that arises from their synergy. The rate processes associated with deposition and diffusion can be quantified in first-principles calculations based on density-functional theory (DFT). In principle, KMC simulations based on DFT can be as accurate as *ab initio* molecular dynamics (MD) with the added benefit that KMC simulations can probe significantly larger length and time scales than *ab initio* MD. However, for many systems of interest, the catalog of DFT rate processes is not sufficiently developed to enable such quantitative simulations.

In this work, we focus on elucidating mechanisms involved in the self-assembly of "nanohuts"[15] in Al(110) homoepitaxy. At temperatures between 330 and 500 K, nanohuts with smooth {111} and {100} facets form and grow to an average height of 50 nm when 30 monolayers (MLs) of Al are deposited on Al(110) with a rate of 1 ML/min.[15] Interestingly, nanohut formation in this homoepitaxial system is driven primarily by kinetic phenomena[16] so detailed studies may reveal insight into kinetic driving forces for assembly. From a fundamental perspective, the current understanding of the diffusion processes that govern self-assembly in multilayer thin-film epitaxy is limited and insights from DFT calculations are useful. As we will elaborate below, Zhu *et al.*[16] used DFT calculations to obtain energy barriers for a variety of different diffusion processes in this system. In the studies reported below, we significantly expand their catalog, by employing DFT calculations to quantify a number of key diffusion mechanisms on the flat, stepped, and faceted surfaces of Al(110) that were not considered by them. In addition to elucidating transport mechanisms for isolated atoms in these different environments, we consider the influence of neighboring atoms on diffusion mechanisms and energy barriers. As we will discuss below, the mechanisms that we find here are critical for describing the formation of self-assembled nanohuts in this and similar systems.

II. METHODS

In the framework of harmonic transition-state theory,[17] which is accurate for low-temperature diffusion on solid surfaces, the rate of adatom hopping from an initial state to a final state via a transition state is given by

$$r = \nu \exp(-E/k_B T), \tag{1}$$

where k_B is the Boltzmann constant, ν is the pre-exponential factor, E is the diffusion-energy barrier, and T is the temperature. Within the harmonic approximation,[17] ν can be obtained using

$$\nu = \frac{\Sigma_{i=1}^{3N} \nu_i}{\Sigma_{i=1}^{3N-1} \nu_i^{\dagger}}, \tag{2}$$

where N is the number of unconstrained atoms and ν_i and $\nu_i^{\dagger}$ are the real, normal-mode frequencies at the minimum and the transition states, respectively. In an extensive theoretical study of adatom surface diffusion, Liu *et al.*[18] found pre-exponential factors in the range of $10^{11}-10^{13}$ s^{-1}, with lower values corresponding to single-atom diffusion processes

(e.g., an adatom hopping on top of the surface) and higher values corresponding to collective diffusion processes, involving the exchange with the substrate. Here, we focus most of our effort on quantifying diffusion-energy barriers, which have a larger effect on the rate than pre-exponential factors. The energy barrier E is given by the difference between the total energies of the initial and transition states. In this work, we obtained these quantities from first-principles total-energy calculations based on DFT, as implemented in the Vienna *ab initio* simulation package (VASP).[19–21] To locate transition states, we employ the climbing-image nudged-elastic band (CI-NEB) method,[22] which is implemented in VASP.

For the DFT total-energy calculations, we used ultrasoft Vanderbilt pseudopotentials,[23] as supplied by Kresse and Hafner,[24] the generalized gradient approximation (GGA) by Perdew and Wang,[25] Fermi-Dirac smearing[26] with a width of 0.2 eV, and an energy cutoff of 129.2 eV. We used the Monkhorst-Pack scheme[27] to sample the Brillouin zone. With a converged $(13\times13\times13)$ **k**-point mesh, we obtained a bulk Al lattice constant of 4.05 Å, which is the same as the experimental value.[28] We also tested a few key results using the GGA by Perdew, Burke, and Ernzerhof[29] with a higher-energy cutoff of 240.3 eV, and confirmed that the energy barriers do not vary significantly.

To model various Al surfaces, we constructed periodic supercells consisting of multilayered slabs with vacuum spacing above the surface. We used vacuum spacings of at least 15 Å, which is sufficient to minimize interactions between the periodic slabs normal to the surface. We adsorbed adatoms on only one side of the slab because the emergence of an artificial electric field perpendicular to the slab due to asymmetry is small for this system.[30–32] To obtain optimized slab geometries, we relaxed the unconstrained atoms until the force on each atom was less than 0.01 eV/Å. Following our previous work for Al(110), we employ a ten-layer slab with the bottom five layers fixed at the bulk positions,[31,32] and for Al(100), we used an eight-layer slab with the bottom four layers fixed at the bulk positions.[32] We selected these as the minimum thicknesses that could accommodate the interlayer relaxations for these surfaces.[31,32] For Al(110), we further tested the slab thickness by performing calculations on 12-layer slabs for two diffusion mechanisms involving exchange of an adatom with the substrate. The energy barriers from these calculations were within 5% of those for ten-layer slabs.

To find the necessary thickness for the Al(111) slabs, we obtained the interlayer relaxations using a 14-layer (1×1) slab. We allowed the top seven layers to relax using a converged $(26\times26\times1)$ **k**-point mesh while keeping the atoms in the bottom seven layers fixed at the bulk positions. We calculated the interlayer relaxation $\Delta_{i,i+1}$, which is the percentage change from the bulk interlayer spacing between layer i and $i+1$, with $i=1$ for the top layer. We obtained $\Delta_{1,2}=+1.08\%$, which is in good agreement with the experimental values of $+0.9\pm0.5\%$ (Ref. 33) and $+1.4\%$ (Ref. 34) from low-energy electron-diffraction (LEED) studies. However, we note that two other LEED studies reported a significantly higher expansion between the first and second layers, with $\Delta_{1,2}=+2.2\%$ (Ref. 35) and $+1.7\pm0.3\%$ (Ref. 36). Our value of $\Delta_{1,2}$ also agrees well with other theoretical estimates based on DFT.[37–42] We obtained $\Delta_{2,3}=-0.38\%$, which is in agreement with the experimental value of $+0.5\pm0.7$ (Ref. 36)—although the experimental value has a large uncertainty. There are also large discrepancies in the values of $\Delta_{2,3}$ predicted in various DFT studies.[37–42] However, these studies all agree on the negative sign of $\Delta_{2,3}$, which implies contraction. The interlayer relaxations for Al(111) are much smaller than what we obtained for Al(110) [$\Delta_{1,2}=-8.61\%$ and $\Delta_{2,3}=+4.92\%$ (Ref. 31)] and Al(100) [$\Delta_{1,2}=+1.76\%$ and $\Delta_{2,3}=+0.67\%$ (Ref. 32)], a trend which is consistent with other experimental and theoretical results.[41,43–45] We found that for Al(111), a six-layer slab with the top three layers unconstrained is sufficient to accommodate the interlayer relaxations, yielding $\Delta_{1,2}=+0.97\%$ and $\Delta_{2,3}=-0.18\%$. Hence, we used this slab thickness for performing further calculations on Al(111).

In previous work,[31,32] we obtained a converged $(5\times4\times1)$ **k**-point mesh for a (5×4) Al(110) slab along the $([1\bar{1}0]\times[001])$ or (in-channel × cross-channel) direction. We use the same or higher **k**-point density for other slabs in this work. The number of atoms per layer in the slabs is large enough to prevent significant lateral interactions between the adatoms in the periodic images of the supercells. To study adatom diffusion on the flat (110) surface, we employed a (5×4) slab with a $(5\times4\times1)$ **k**-point mesh. We used an (8×3) slab with a $(4\times6\times1)$ **k** mesh to study (100) steps and facets, and a (4×6) slab with a $(7\times3\times1)$ **k**-point mesh to study (111) steps and facets on Al(110). For adatom diffusion on the flat (100) and (111) surfaces, we employed a (5×5) slab with a $(5\times5\times1)$ **k**-point mesh, and a (4×4) slab with a $(7\times8\times1)$ **k**-point mesh, respectively.

To find transition states using the CI-NEB method, we relaxed two slabs with atomic configurations corresponding

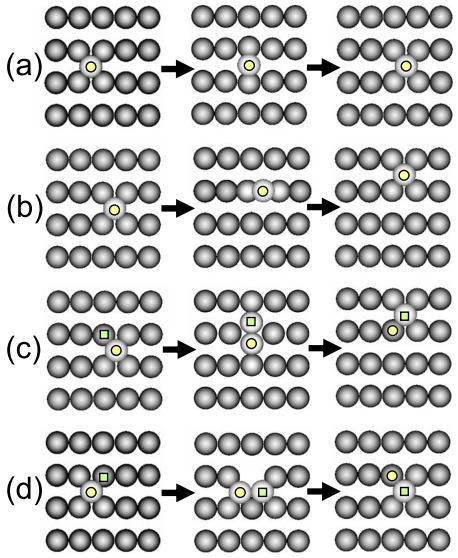

FIG. 1. (Color online) Atomic configurations (top view) of the initial (left), transition (center), and final (right) states proposed by Stumpf and Scheffler (Ref. 30) for adatom diffusion on the flat Al(110) surface via (a) in-channel hopping; (b) cross-channel hopping; (c) cross-channel exchange and; (d) in-channel exchange. Initial adatoms are labeled by circles and substrate atoms involved in the exchange mechanisms are labeled by squares.

TABLE I. Energy barriers obtained in this work for Al adatom diffusion on the flat Al surfaces shown in Figs. 1, 3, and 4, along with the results from other studies.

		Energy barriers (eV)		
Move	Figure	This work	Previous work (theory)	Experiments
Al(110)				0.43[d]
1. ⟨110⟩ hopping	1(a)	0.47	0.60,[a] 0.38[c]	
2. ⟨001⟩ hopping	1(b)	0.71	1.06,[a] 0.83[c]	
3. ⟨110⟩ exchange	1(d)	0.39	0.33,[a] 0.33[b]	
4. ⟨001⟩/⟨110⟩/⟨112⟩ exchange	1(c) 3(a)–3(c)	0.38	0.62,[a] 0.49[b]	
5. ⟨112⟩ exchange	3(d)	0.33	0.50[c]	
Al(100)				
1. Hop	4(a)	0.57	0.69,[a] 0.46,[c] 0.65,[e] 0.51,[f] 0.55[g]	
2. Exchange	4(b)	0.51		
3. Exchange	4(c)	0.22	0.40,[a] 0.19,[b]0.17[c] 0.20,[e] 0.16[g]	
Al(111)				0.042 ± 0.004 [i]
1. hcp to fcc	4(d)	0.05	0.04[a–c,h]	
2. fcc to hcp	4(d)	0.01		

[a]Reference 30.
[b]Reference 16.
[c]Reference 48.
[d]Reference 51.
[e]Reference 63.
[f]Reference 64.
[g]Reference 65.
[h]Reference 66.
[i]Reference 67.

to the desired initial and final states. Then, we constructed three (unless stated otherwise) intermediate states or "images" between them, following an initial guess of the diffusion mechanism. In CI-NEB calculations, the positions of the atoms are optimized so that the images follow a minimum-energy pathway (MEP) while also forcing the image with the highest energy to reside at the transition state. This offers an advantage over the regular NEB method,[46] which finds the MEP but does not guarantee that the highest-energy image is the transition state. In NEB calculations, a sufficient number of images is needed to obtain a good estimate of the MEP so that a good transition state can be found. However, we can obtain the transition states directly and accurately by employing much fewer images with the CI-NEB method. Interestingly, even one image was found to be sufficient for most of the calculations in this work, except for a case with two transition states between the initial and final states, as discussed below.

III. RESULTS

A. Diffusion on Al(110), Al(100), and Al(111)

Adatom diffusion on Al(110) has been investigated in previous theoretical studies using semiempirical potentials[18,47] and DFT calculations.[16,30,48] However, even among the DFT studies, there is no consensus regarding the dominant diffusion mechanisms and their energy barriers. For adatom diffusion on Al(110), we first investigated the mechanisms proposed by Stumpf and Scheffler.[30] In Fig. 1, we show the atomic configurations that we obtained following their proposed hopping [Figs. 1(a) and 1(b)] and exchange [Figs. 1(c) and 1(d)] mechanisms. Our energy barriers for these mechanisms, along with those from previous DFT studies, are shown in Table I.

We found an energy barrier of 0.47 eV for in-channel hopping [cf., Fig. 1(a)] and 0.71 eV for cross-channel hopping [Fig. 1(b)]. Our barriers have approximately two-thirds of the magnitudes of those reported by Stumpf and Scheffler,[30] perhaps because they used the local-density approximation (LDA) while we used the GGA. Deviations from the hopping barriers obtained by Sun *et al.*[48] are probably due to the thinness of their Al(110) slab (four layers), which is not sufficient to account for the interlayer relaxations associated with this surface.[31] We also matched Stumpf and Scheffler's proposed[30] transition state for cross-channel exchange, shown in Fig. 1(c). For this mechanism, we obtained an energy barrier of 0.38 eV, which is significantly smaller than values reported in previous work.[16,30] As discussed above, Stumpf and Scheffler used the LDA, which

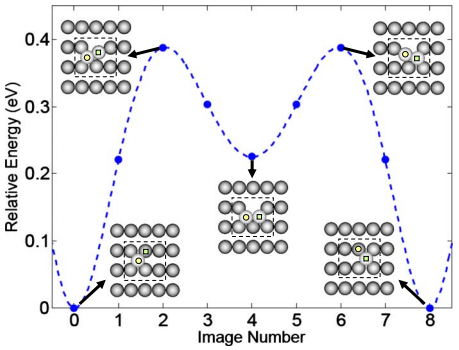

FIG. 2. (Color online) The MEP and atomic configurations (top view for images 0, 2, 4, 6, and 8) for the in-channel exchange mechanism shown in Fig. 1(d). Images 2 and 6 are the transition states, image 4 is the intermediate state, and images 0 and 8 are the initial and final states, respectively. The initial adatom is labeled by a circle and the substrate atom involved in the exchange mechanism is labeled by a square.

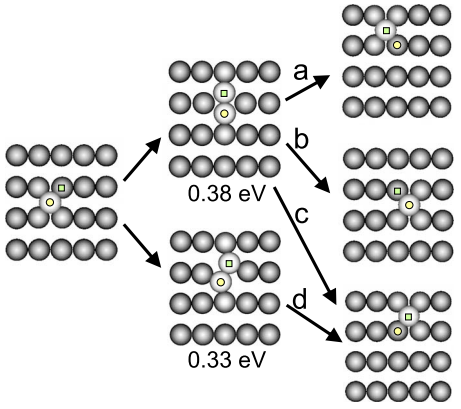

FIG. 3. (Color online) Atomic configurations (top view) of the initial (left), transition (center), and final (right) states, along with energy barriers for the dominant adatom diffusion mechanisms on Al(110): (a) cross-channel exchange; (b) in-channel exchange; (c) diagonal exchange; and (d) alternate diagonal exchange. The initial adatom is labeled by a circle and the substrate atom involved in the exchange mechanism is labeled by a square.

may be the reason for our discrepancy with them. Surprisingly, our diffusion barrier for cross-channel exchange does not agree with that reported by Zhu *et al.*,[16] even though they used the same GGA and slab thickness. The only known difference is that we employed the CI-NEB method to find diffusion barriers while they used the NEB method. As discussed above, it is possible that we located the transition state more precisely with this method and, hence, we found a more accurate energy barrier.

Moving on to in-channel exchange, we found that the transition state proposed by Stumpf and Scheffler,[30] shown in Fig. 1(d), is actually an intermediate local minimum and that this mechanism proceeds via a move from the initial state to the intermediate state followed by a second move from the intermediate state to the final state. To confirm the locations of the transition states, we performed two separate CI-NEB calculations between the initial and intermediate states, and between the intermediate and final states. The MEP for this mechanism and the atomic configurations of the key images are shown in Fig. 2.

Since in-channel exchange occurs as a result of two separate, sequential moves, the net rate for this process is given by the mean first-passage time.[49] For the mechanism in Fig. 2, we obtained the mean first-passage time τ for moving from the initial state to the final state, considering one or more visits to the intermediate state and possibly multiple revisits to the initial state.[49] This is given by

$$\tau = \frac{r_1 + 2r_2}{r_1 r_2}, \tag{3}$$

where r_1 is the rate from the initial state to the intermediate state and r_2 is the rate from the intermediate state to either the final or initial state. These have the form given by Eq. (1) with $E_1 = 0.39$ eV and $E_2 = 0.16$ eV. The attempt frequencies ν_1 and ν_2 are given by Eq. (2). We conducted dynamical matrix calculations[17] in VASP to obtain the normal-mode frequencies for ν_1 and ν_2. We displaced seven atoms (enclosed inside the dashed areas in Fig. 2) from their equilibrium positions by ± 0.005 Å in the direction of each Cartesian coordinate in relaxed slabs of the initial, transition, and intermediate states. We found one imaginary normal-mode frequency at the transition state, and obtained the attempt frequencies $\nu_1 = 3.97 \times 10^{12}$ s^{-1} and $\nu_2 = 3.70 \times 10^{12}$ s^{-1} using Eq. (2). The rate of the effective move is given by $1/\tau$. By representing this effective rate in the form of the Arrhenius equation, i.e.,

$$1/\tau = \nu_{eff} \exp(-E_{eff}/k_B T), \tag{4}$$

we obtained the energy barrier E_{eff} and attempt frequency ν_{eff} of the effective move from the slope and y intercept of an Arrhenius plot of $\ln(1/\tau)$ vs $1/T$. In the temperature range between 200 and 500 K, this yields $\nu_{eff} = 1.980 \times 10^{12}$ s^{-1} and $E_{eff} = 0.39$ eV. We note that the value of this effective barrier is higher than those found by Stumpf and Scheffler[30] and by Zhu *et al.*,[16] who both assumed that the intermediate local minimum was the transition state.

There is an alternate and slightly more favorable mechanism for diffusion in the in-channel direction, shown as move *b* in Fig. 3. This move has the same transition state as that for cross-channel exchange (move *a* in Fig. 3) and the same energy barrier of 0.38 eV. The symmetric transition state for these moves can also lead to diffusion in the $[1\bar{1}2]$ (diagonal) direction with the same energy barrier, shown as move *c* in Fig. 3.

In separate work, we studied diffusion mechanisms on Al(110) using accelerated *ab initio* MD simulations.[50] In that study, we found that the most dominant mechanism for adatom diffusion is a diagonal exchange, shown as mechanism *d* in Fig. 3. Experimental studies on the (110) surfaces of Al, Ni, Ir, and Pt have shown that the energy barrier for adatom diffusion along the cross-channel direction is lower than or comparable to that for the in-channel direction.[51–54] However, theoretical studies before our work indicate the opposite behavior on Al(110) and other fcc(110) surfaces.[16,18,30,47,48,55–61] Using Cl-NEB calculations on

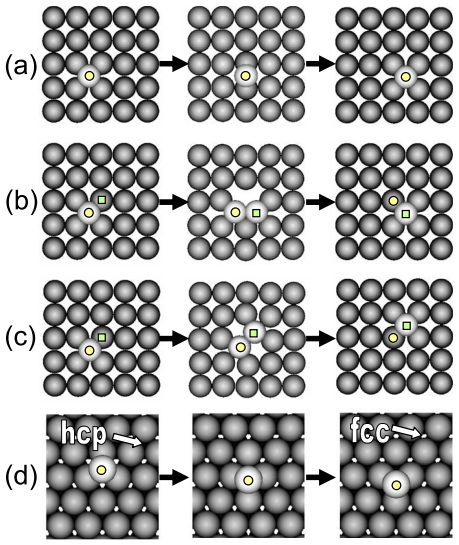

FIG. 4. (Color online) Atomic configurations (top view) of the initial (left), transition (center), and final (right) states for (a) Al(100) hopping; (b) Al(100) exchange; (c) Al(100) diagonal exchange; and (d) Al(111) hopping from an hcp to a fcc site. Initial adatoms are labeled by circles and the substrate atoms involved in the exchange mechanisms are labeled by squares.

Al(110), we obtained an energy barrier of 0.33 eV for the diagonal exchange mechanism, which has the transition state shown in *d* in Fig. 3. This mechanism was not considered in most of the previous theoretical studies on Al(110).[16,18,30,47] Sun *et al.*[48] studied this mechanism on Al(110) but found it to be significantly less feasible than the in-channel hopping mechanism—perhaps because of the thinness of their slabs. Hence, we match the experimental trends by finding that the lowest diffusion barrier for an isolated adatom on Al(110) is that for diagonal motion, which advances the atom in both the in-channel and cross-channel directions. In a recent study of diffusion on Cu(110),[62] the energy barrier for the diagonal exchange mechanism was found to be close to that for the in-channel hopping mechanism.

For adatom diffusion on Al(100), we studied one hopping and two exchange mechanisms, which are shown in Fig. 4. We obtained an energy barrier of 0.57 eV for the hopping mechanism shown in Fig. 4(a). For the exchange mechanisms shown in Figs. 4(b) and 4(c), we find energy barriers of 0.51 eV and 0.22 eV, respectively. Our values for these barriers are in good agreement with those in other DFT studies,[30,48,63–65] as shown in Table I. On Al(111), we found that the hcp binding sites are more stable (by ~0.04 eV) than the fcc sites. An adatom can hop from an hcp site to a nearest-neighbor fcc site with an energy barrier of 0.05 eV and the transition state shown in Fig. 4(d). The energy barrier for an adatom to hop from an fcc site to a nearest-neighbor hcp site is only 0.01 eV. These values are in good agreement with other theoretical[16,30,48,66] and experimental results,[67] reported in Table I.

B. Diffusion in the vicinity of (100) and (111) steps on Al(110)

In the initial stages of thin-film epitaxy, single-layer islands form, whose steps may have various orientations. The upward/downward motion of atoms over the step edges can significantly influence the morphology of a growing film. Generally, the energy barriers for atoms to descend step edges are higher than those on the flat terrace. The excess barrier to descend the step edge is referred to as the Ehrlich-Schwoebel (ES) barrier.[68,69] A high ES barrier promotes atoms to stay and nucleate on top of islands whereas a low ES barrier allows the atoms to descend the steps, thereby promoting layer-by-layer growth.

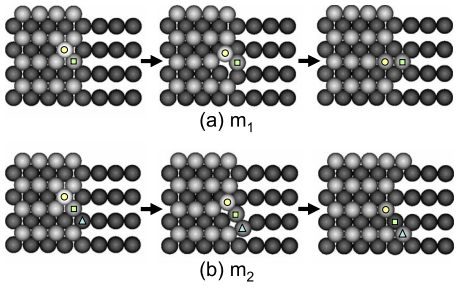

FIG. 5. (Color online) Atomic configurations (top view) of the initial (left), transition (center), and final (right) states for interlayer diffusion on the (100) step: (a) proposed by Zhu *et al.* (Ref. 16) and (b) proposed in this work. Initial adatoms are labeled by circles and atoms involved in the exchange mechanisms are labeled by squares and triangles.

We studied the (100) and (111) steps, which are the most stable on Al(110).[32] We constructed (100) steps as one-layer-high islands that are four atoms wide along the in-channel and infinite along the cross-channel direction and (111) steps that are three atoms wide along the cross-channel and infinite along the in-channel direction, as shown in Figs. 5 and 6. Zhu *et al.*[16] proposed the exchange mechanisms m_1 in Fig. 5(a) for upward/downward diffusion on the (100) step and m_3 in Fig. 6(a) for the (111) step. For mechanisms m_1 and m_3, we found energy barriers of 0.58 eV (0.44 eV) and 0.65

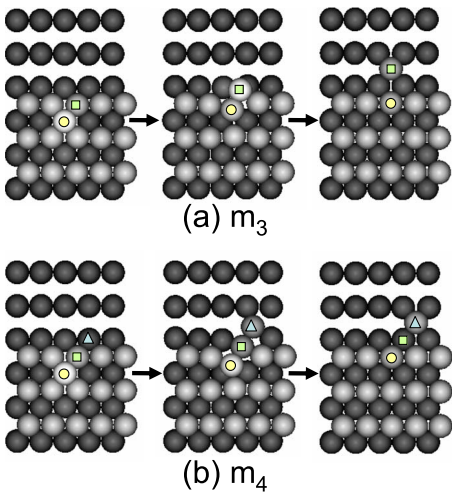

FIG. 6. (Color online) Atomic configurations (top view) of the initial (left), transition (center), and final (right) states for interlayer diffusion on the (111) step: (a) proposed by Zhu *et al.* (Ref. 16) and (b) proposed in this work. Initial adatoms are labeled by circles and atoms involved in the exchange mechanisms are labeled by squares and triangles.

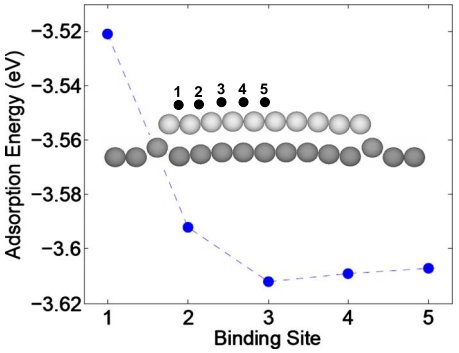

FIG. 7. (Color online) Adsorption energies on top of a one-layer-high island at different binding sites (1–5) close to the (100) step edge on Al(110). The relaxed positions (side view) of the atoms forming the substrate (dark) and the island (light) are shown (not-to-scale in the vertical direction), along with the binding sites on top of the island, which are indicated by black circles.

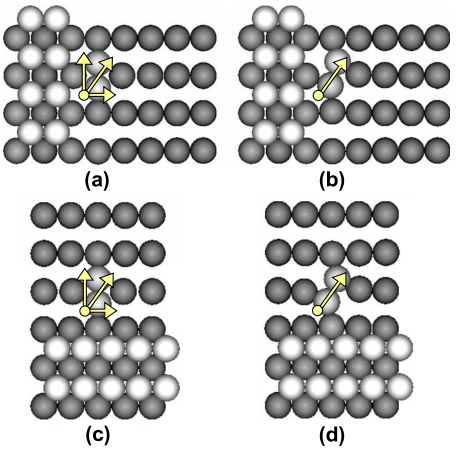

FIG. 8. (Color online) Transition states for adatom diffusion near steps formed by one-layer-high islands on Al(110), using the exchange mechanisms shown in Fig. 3, for (a) cross-channel, in-channel, or diagonal moves adjacent to the (100) step; (b) alternate diagonal move adjacent to the (100) step; (c) cross-channel, in-channel, or diagonal moves adjacent to the (111) step; and (d) alternate diagonal move adjacent to the (111) step. The arrows begin at the initial states and point to possible final positions.

eV (0.68 eV), respectively, for the upward (downward) transport of adatoms. These values are in good agreement with those reported by Zhu *et al.*[16] The upward diffusion of adatoms over steps is generally considered to be less feasible than downward diffusion. Interestingly, however, our results confirm those of Zhu *et al.*,[16] who found that the energy barrier for upward diffusion is slightly smaller than that for downward diffusion on the (111) step.

In addition to confirming the results of Zhu *et al.*,[16] we found two, three-atom exchange mechanisms, m_2 in Fig. 5(b) and m_4 in Fig. 6(b), that are more complex but kinetically more feasible than the two-atom exchange mechanisms (m_1 and m_3). The energy barriers for upward (downward) transport via these mechanisms are 0.49 eV (0.36 eV) for m_2 and 0.58 eV (0.62 eV) for m_4. In a simplified definition,[70] the ES barrier E_{ES} is given by $E_{\mathrm{ES}}=E_s-E$, where E is the energy barrier for diffusion on the terrace and E_s is the barrier for interlayer transport of adatoms down the step edges. Taking $E=0.33$ eV for terrace diffusion, we find that E_{ES} for the (111) step (0.29 eV) is high but that for the (100) step (0.03 eV) is small. In this scenario, atoms on the (110) terrace on the top of an island will not frequently descend the (111) steps, but have an easy passage down the (100) steps. This suggests that layer-by-layer growth is likely during Al(110) homoepitaxy, in contradiction to the experimental findings.[15]

To resolve the apparent contradiction with experiment, we need to account for other origins of the ES barrier, which reflects the approach of atoms to a step edge, as well as their descent over the edge. Thus, we consider the approach of an atom from the center of an island to the edge. For this study, we constructed a one-layer-high island, which is ten atoms wide along the in-channel and infinite along the cross-channel direction, on a (13×2) Al(110) slab, as shown in Fig. 7. Using a $(2\times10\times1)$ **k**-point mesh, we obtained adsorption energies of an adatom on five, fourfold hollow sites (Fig. 7) as the atom approaches the (100) edge. Here, we define the adsorption energy as the difference between the energies of the slab (including the island) with and without the adatom. Figure 7 also shows the values of the adsorption energies at these binding sites, which are significantly smaller in magnitude for the two edge sites (1 and 2) than for the center sites (3, 4, and 5). In a preliminary study, we found that this edge effect is negligible for the (111) step on Al(110), thus we did not perform an elaborate investigation for this step.

The adsorption-energy profile in Fig. 7 can be attributed to alterations in the electronic charge density and strain effects that occur close to the (100) step edge. The strain effect is evident in Fig. 7 from different vertical relaxations of the atoms forming the substrate and the island close to the (100) edge. Adatoms on the top Al(110) terrace have to climb uphill energetically when diffusing from the center to the (100) edge and would prefer to stay on the more stable sites in the center. In field-ion microscopy studies on Pt(111) (Ref. 71) and Ir(111),[72] an excluded zone with a reduced population of adatoms was observed close to descending step edges, suggesting the same behavior. Also, in other theoretical studies of fcc(111) surfaces, changes in adsorption energies have been reported up to several sites away from the descending step edge.[73,74] Thus, hindered diffusion from the center of an island to the (100) step edge and a high-energy barrier for descending the (111) step lead to high effective ES barriers that promote three-dimensional growth in Al(110) homoepitaxy.

To accurately describe the lateral growth and decay of islands, we obtained energy barriers for an Al adatom to move along, away from, and toward the (100) and (111) steps on the lower Al(110) terrace. For these calculations, we used slabs with two-atom-wide (semi-infinite) islands to simulate steps, as shown in Fig. 8, which is sufficient according to our previous study.[32] Using hopping mechanisms similar to those shown in Figs. 1(a) and 1(b), an adatom can move along the (100) step with an energy barrier of 0.66 eV, and away from (toward) the (100) step with an energy barrier of 0.57 (0.42) eV. Similarly, an adatom can hop along the

(111) step with an energy barrier of 0.47 eV and away from (toward) the (111) step with an energy barrier of 0.73 (0.75) eV. Using exchange mechanisms similar to those shown in Figs. 3(a)–3(c), an adatom can move along and away from (toward) the (100) step with the same transition state shown in Fig. 8(a) and an energy barrier of 0.46 (0.31) eV, and similarly, along and away from (toward) the (111) step with an energy barrier of 0.36 (0.38) eV and the transition state shown in Fig. 8(c). An alternate mechanism to move away from (toward) the steps is similar to that shown in Fig. 3(d), with an energy barrier of 0.49 (0.34) eV for the (100) step and 0.29 (0.31) eV for the (111) step, and the transition states shown in Figs. 8(b) and 8(d), respectively. We note that the mechanisms discussed above involve an exchange of the adatom with a substrate atom that is not directly bonded to atoms in the step. Our preliminary results indicate that exchange between substrate atoms that are bonded to the step results in significantly higher-energy barriers than those reported above.

Many of the mechanisms shown in Fig. 8 were also probed by Zhu *et al.*[16] and, in all cases, our energy barriers are comparable to theirs. Zhu *et al.* used wider steps than us, which also validates our use of two-atom-wide steps for these calculations. However, they concluded that the in-channel hopping mechanism has the lowest-energy barrier to move away from or toward the (100) steps, whereas, we found that the exchange mechanism with the transition state shown in Fig. 8(a) is most favorable for this move. For (100) steps, it is easier for an adatom to join the step than to move away. In contrast, for (111) steps, it is easier to move away from the step than to join it. This kinetic anisotropy can have a significant influence on the aspect ratios of self-assembled structures during homoepitaxial growth on Al(110).

C. Transport between (110), (100), and (111) facets

During homoepitaxial growth on Al(110), nanostructures are formed that have (111) and (100) facets.[15] Atoms can climb onto these facets from the bottom (110) terrace or move down onto them from the upper (110) terrace, by crossing edges where the (110) and the (100)/(111) facets merge (edge-crossing moves). Similarly, adatoms can move from the (100) to the (111) facet and vice versa via corner-crossing moves. Atoms are also deposited directly onto the (100) and (111) facets during growth. A net accumulation of atoms on the facets, leading to facet growth, is strongly dependent on their relative rates of arrival and departure on the facets. To study the mechanisms and kinetics of the edge-crossing moves, we constructed Al(110) slabs containing multilayer islands with four- or five-atom-wide bases that were infinite along the cross-channel direction for (100) facets and infinite along the in-channel direction for (111) facets, as shown in Figs. 9 and 10, respectively. To study corner-crossing moves, we constructed a (6×4) Al(100) slab with a three-layer-high island, which was five atoms wide and infinitely long, as shown in Fig. 11, forming lower and upper (100) terraces and (111) facets on the sides.

Stable binding sites on the (100) facet occur for islands with two or more layers. Using the hopping mechanism m_5 in Fig. 9(a), an adatom can climb from the bottom (110) terrace to the (100) facet. The place-exchange mechanism m_6 in Fig. 9(b) leads to transport from the (100) facet to the top

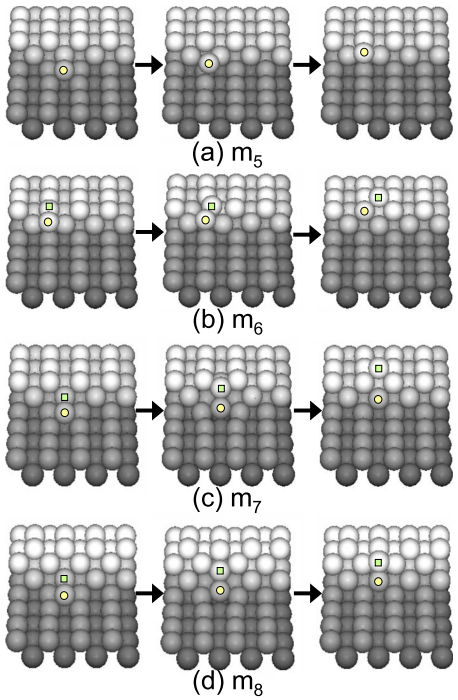

FIG. 9. (Color online) Atomic configurations [view facing the (100) facet] obtained in this work at the initial (left), transition (center), and final (right) states for (a) hopping from the bottom (110) terrace to the (100) facet; (b) exchange from the (100) facet to the top (110) terrace; (c) exchange from the bottom to the top (110) terrace for two-layer-high islands; and (d) exchange from the bottom (110) terrace to the (100) facet on three layer and higher islands. Initial adatoms are labeled by circles and atoms involved in exchange mechanisms are labeled by squares.

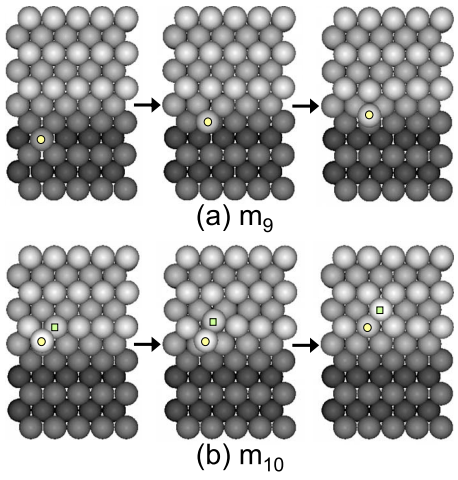

FIG. 10. (Color online) Atomic configurations (top view) of the initial (left), transition (center), and final (right) states for (a) hopping from the bottom (110) terrace to the (111) facet and (b) exchange from the (111) facet to the top (110) terrace. Initial atoms are labeled by circles and atoms involved in the exchange mechanisms are labeled by squares.

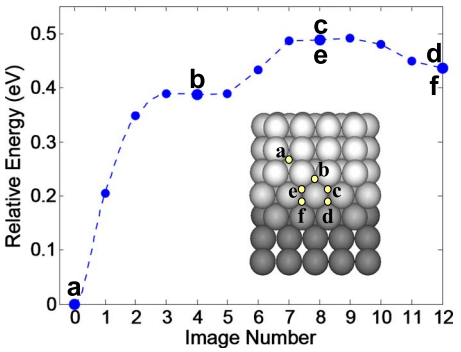

FIG. 11. (Color online) The minimum-energy pathways for different moves relevant for atomic diffusion between the (100) and (111) facets. Images denoted by $a-f$ (large markers) are the fixed local minima, and the intermediate images (small markers) were obtained from CI-NEB calculations using neighboring local minima as the initial and final states. The relevant binding sites are shown on a slab with a three-layer-high island on Al(100) [view facing the (111) facets].

(110) terrace. On two-layer-high islands, an atom can move directly from the bottom (110) terrace to the top (110) terrace using the exchange mechanism m_7 shown in Fig. 9(c). On three-layer and higher islands, adatoms can move from the bottom (110) terrace to the (100) facet using a similar mechanism m_8 in Fig. 9(d). The energy barriers that we obtained for these mechanisms are shown in Table II, along with those obtained by Zhu *et al.*,[16] for comparison. Our energy barriers for three-layer-high islands are in good agreement with those reported by Zhu *et al.*, who used a vicinal surface equivalent to a six-layer-high island. However, they did not report the energy barrier for the hopping mechanism m_5 and they did not consider mechanism m_7 for two-layer-high islands. Because of their moderate energy barriers, these two mechanisms are expected to increase the frequency of (100)-facet-climbing moves, particularly in the early stages of facet formation.

Proceeding to the (111) facet, we found that fcc sites [binding site for the adatom at the final state in Fig. 10(a)] are the only stable binding sites next to the ascending edge. The fcc sites are also more stable than the hcp sites on the (111) facet next to the descending edge [binding site for the adatom at the initial state in Fig. 10(b)], with a difference in adsorption energy of ~0.01 eV. This is in contrast to the (111) terrace, where the hcp site is preferred. Unlike the (100) facets, stable binding sites are available on (111) facets that are only one layer high. In Figs. 10(a) and 10(b), we show the dominant mechanisms for moves from the bottom (110) terrace to an fcc site on the (111) facet (m_9), and a move from an fcc site on the (111) facet to the top (110) terrace (m_{10}). The energy barriers we obtained for these mechanisms are reported in Table II. We found that the energy barrier for m_9 on the one-layer-high island is significantly lower than that for the higher islands. This, along with the mechanism m_7 on the (100) facet, would make it easier for an adatom to ascend the facets during the initial stages of nucleation, thus facilitating the formation of three-dimensional structures. Similar variations in energy barriers for islands with small heights have been reported in the past.[75–77]

TABLE II. The energy barriers (in eV) for the upward (E_{up}) and downward (E_{down}) transport of adatoms using the mechanisms shown in Figs. 9–11 on islands with different numbers of atomic layers N. Where possible, the values obtained by Zhu *et al.* (Ref. 16) are shown for comparison.

Mechanism	N	E_{up}	E_{down}
(100) facet			
m_5	2	0.69	0.31
	3	0.67	0.32
m_6	2	0.13	0.26
	3	0.13	0.26
	6[a]	0.13	0.33
m_7	2	0.55	0.29
m_8	3	0.65	0.28
	6[a]	0.69	0.18
(111) facet			
m_9	1	0.65	0.07
	2	0.72	0.07
	3	0.71	0.05
	4[a]	0.70	0.03
m_{10}	1	0.07	0.69
	2	0.07	0.69
	3	0.08	0.68
	4[a]	0.04	0.69
(100)-(111) facet			
m_{11}	3	0.05[(111)→(100)]	0.49[(100)→(111)]
	not known[a]	0.08[(111)→(100)]	0.53[(100)→(111)]

[a]Reference 16.

Finally, we obtained energy barriers for corner-crossing moves between the (100) and (111) facets. We found that place exchange is the most feasible mechanism for an adatom to move diagonally between site a on the (100) facet to site b on the (111) facet, shown in Fig. 11. Figure 11 also shows the MEP for this mechanism, indicating a negligible barrier to move from site b to site a. Although our calculations show that site b is stable, the MEP suggests that it is a shallow minimum and effectively unstable. Thus, we conducted a separate CI-NEB calculation for hopping between site b and site c (same as e) in Fig. 11. The MEP for this move is appended to the MEP for the previous move ($a \rightarrow b$). Again, we found that site c (or e) is a shallow minimum and is also effectively unstable. Further away from the (100)-(111) edge, we found that site d (or f) is stable, and the MEP for hopping between sites c and d (e and f) is appended in Fig. 11. Hence, two closest sites on Al(111) next to the (100)-(111) edge are effectively unstable, and the net corner-crossing move proceeds from site a to $d(a \rightarrow b \rightarrow c \rightarrow d)$ or a to $f(a \rightarrow b \rightarrow e \rightarrow f)$ with an energy barrier of 0.49 eV and 0.05 eV for the reverse move. Our barriers for corner-crossing moves are in good agreement with those reported by Zhu *et al.*[16]

D. Effect of neighboring atoms on energy barriers

Neighboring atoms can modify the energy barriers for the atomic diffusion moves discussed above. For a diffusion

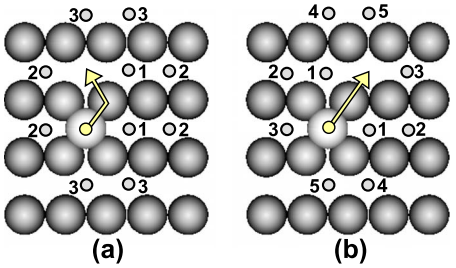

FIG. 12. (Color online) The binding sites for a neighboring atom (shown by small circles in a top view) for which we obtained ΔE_T for: (a) diffusion mechanisms in Figs. 3(a)–3(c) and 3(b) diffusion mechanism in Fig. 3(d). Binding sites that have equivalent transition states have the same number.

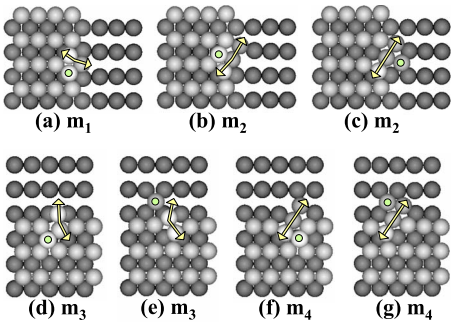

FIG. 13. (Color online) Atomic configurations (top view) obtained at the transition states for different mechanisms (in Figs. 5 and 6) for interlayer transport of adatoms on the (100) step [(a)–(c)] and the (111) step [(d)–(g)] on Al(110), in the presence of a neighboring atom (labeled by a circle). Arrows indicate the initial and final positions of the diffusing atoms.

mechanism i, the energy barrier E^i in the presence of neighboring atoms can be represented in terms of the energy barrier E_o^i for an isolated adatom and the atomic interactions from the neighbors at the initial ΔE_I and the transition ΔE_T^i states, i.e., $E^i = E_o^i + \Delta E_T^i - \Delta E_I$. ΔE_I can be estimated using the lattice-gas model or the connector model,[32] which we developed recently to efficiently capture many-body atomic interactions on surfaces. We performed extensive calculations of atomic interactions between Al adatoms on Al(110) (Refs. 31 and 32) and Al(100) (Ref. 32) in previous work. It is a common practice to neglect ΔE_T^i and estimate the unknown energy barriers as $E^i = E_o^i - \Delta E_I$. We refer to this as the bond-breaking model.[78–80] Fichthorn and Scheffler[81] approximated ΔE_T^i by averaging atomic interactions at the initial and final states, and obtained the unknown barrier as $E^i = E_o^i + (\Delta E_I + \Delta E_F)/2 - \Delta E_I$. We refer to this as the interpolation model.

Limiting our study to the effect of one neighboring atom, we first considered diffusion on the (110) terrace and obtained the transition-state interactions for the exchange mechanisms with an adatom in each of the positions in Fig. 12. We performed CI-NEB calculations to obtain the total energy of the transition state E_T^i for mechanism i. The atomic interactions at the transition state are given by $\Delta E_T^i = E_T^i - E_{To}^i - E_{ads}$, where E_{To}^i is the energy of the transition state for an isolated atom undergoing mechanism i and E_{ads} is the adsorption energy of an isolated adatom at the site occupied by the neighbor [e.g., the fourfold site on the Al(110) terrace].

Table III shows the values of ΔE_T for the different sites shown in Fig. 12. The magnitudes of ΔE_T are significant, especially for sites 1 and 2 in Fig. 12(a) and sites 3 and 5 in Fig. 12(b). These indicate the error in using the bond-breaking model, which ignores transition-state interactions. We note that the interpolation model is not well defined for the configurations shown in Fig. 12(a) because there are different initial and final states that correspond to the same transition-state configurations, which erroneously yield different values for the transition-state interactions.

To study short-range, transition-state interactions on (100) and (111) steps and facets, we considered the mechanisms and positions of neighboring atoms shown in Figs. 13 and 14, respectively. The values of ΔE_T for these cases, along with the diffusion-energy barriers for these moves are reported in Table IV. For most cases in Figs. 13 and 14, a neighboring atom induces attraction at the transition states. The actual energy barriers for upward and downward transport depend on the combined effects of interactions at both the initial and transition states. In some configurations, attractive interactions at the transition states decrease the energy barriers significantly, even when there are negligible interactions at the initial states. This occurs for the downward moves in Figs. 13(e) and 13(g), as well as for the upward moves in Fig. 13(f) and Figs. 14(a), 14(c), and 14(g), where the reduction in the energy barrier is equal to ΔE_T. Interestingly, for some configurations the energy barriers are dominated by transition-state interactions and are lowered even when the interactions at the initial states are strongly attractive. This occurs for upward moves in Figs. 14(e) and 14(f), where we see a significant reduction in the energy barriers for (111)-facet climbing moves. Also for the (100) facet, the energy barrier for the facet-climbing mechanism m_5 is significantly reduced in Figs. 14(a) and 14(c). These results indicate that facet-climbing moves are easier for a dimer than for a single atom. Previous theoretical studies

TABLE III. Interaction energies at the transition states ΔE_T (in eV) for the configurations and adsorption sites shown in Fig. 12.

	ΔE_T				
Figure	Site 1	Site 2	Site 3	Site 4	Site 5
12(a)	0.05	−0.04	0.00		
12(b)	0.00	0.02	0.04	0.01	0.03

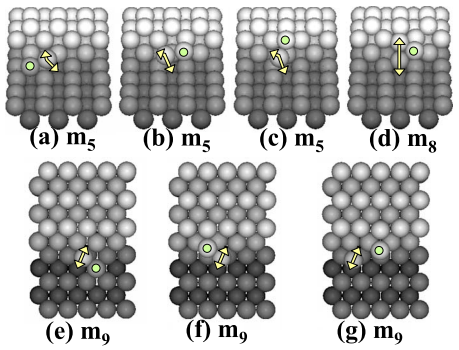

FIG. 14. (Color online) Atomic configurations obtained at the transition states for different mechanisms (in Figs. 9 and 10) for edge-crossing moves on the (100) facet [(a)–(d)] (a view facing the facet) and the (111) facet [(e)–(g)] (top view) on Al(110), in the presence of a neighboring adatom (labeled by a circle) at different positions. Arrows indicate the initial and final positions of the diffusing atoms.

have shown that a dimer can also diffuse easily on the (111) (Refs. 66 and 82) and (100) (Ref. 82) surfaces of Al.

IV. CONCLUSIONS

Using CI-NEB method based on DFT, as implemented in VASP, we obtained diffusion-energy barriers adatoms on the flat (110), (100), and (111) surfaces of Al, the (100) and (111) steps on Al(110), and between the Al(100), Al(111), and Al(110) facets. We found that atoms prefer to move diagonally on Al(110) using an exchange mechanism between the adatom and a substrate atom. Adatom diffusion is isotropic via this mechanism, in agreement with experimental studies of diffusion on fcc(110) surfaces.[51–54] Similarly, we found that diagonal exchange involving three atoms is the dominant mechanism for interlayer transport on the (100) and (111) steps on Al(110). We find that the origin of ES barrier to descend the (100) step is hindered diffusion to the step edge while for the (111) step, the ES barrier originates from the large energy barrier to descend the step edge. For (100) steps, it is easier for an adatom to join the step than to move away. In contrast, for (111) steps, it is easier to move away from the step than to join it. This kinetic anisotropy can have a significant influence on the aspect ratios of self-assembled structures during homoepitaxial growth on Al(110). The hopping and exchange mechanisms are approximately equally feasible for atoms to ascend the (100) facet from the (110) surface. For two-layer-high islands, an additional channel is available for atoms to ascend from the lower to the upper (110) terrace in a single move via the (100) facet, which promotes the formation of three-dimensional nanostructures. The energy barriers for atoms to ascend/descend small (100) and (111) facets depend on the height of the facet. We studied how a neighboring adatom influences the energy barrier for various types of diffusion moves. A significant finding is that it is easier for a dimer to climb from a (110) terrace to the (100) and (111) facets than it is for an isolated adatom. Taken together, the energy barriers obtained in this work indicate trends that lead to the formation of faceted, three-dimensional nanohuts in homoepitaxial growth on Al(110).

TABLE IV. Interaction energies at the transition states ΔE_T (in eV) for the mechanisms and the positions of neighboring atoms in Figs. 13 and 14. The corresponding energy barriers for upward and downward moves in the absence (E^o_{up}, E^o_{down}) and presence (E_{up}, E_{down}) of a neighboring atom are also shown.

Mechanism (E^o_{up}, E^o_{down})	Figure	ΔE_T	(E_{up}, E_{down})
m_1 (0.58, 0.44)	13(a)	−0.03	(0.59, 0.37)
m_2 (0.49, 0.36)	13(b)	−0.05	(0.48, 0.27)
	13(c)	0.16	(0.65, 0.56)
m_3 (0.65, 0.68)	13(d)	0.00	(0.65, 0.83)
	13(e)	−0.08	(0.73, 0.60)
m_4 (0.58, 0.62)	13(f)	−0.08	(0.50, 0.69)
	13(g)	−0.10	(0.63, 0.52)
m_5 (0.67, 0.32)	14(a)	−0.20	(0.47, 0.31)
	14(b)	−0.11	(0.75, 0.22)
	14(c)	−0.11	(0.56, 0.46)
m_8 (0.65, 0.28)	14(d)	−0.06	(0.77, 0.47)
m_9 (0.72, 0.07)	14(e)	−0.39	(0.50, 0.08)
	14(f)	−0.47	(0.65, 0.01)
	14(g)	−0.07	(0.63, 0.40)

ACKNOWLEDGMENT

This work has been supported by the National Science Foundation under Grant No. DMR 0514336.

*fichthorn@psu.edu

[1] F. Buatier de Mongeot, A. Toma, A. Molle, S. Lizzit, L. Petaccia, and A. Baraldi, Nanoscale Res. Lett. **2**, 251 (2007).
[2] T. E. Madey, W. Chen, H. Wang, P. Kaghazchi, and T. Jacob, Chem. Soc. Rev. **37**, 2310 (2008).
[3] K. Brunner, Rep. Prog. Phys. **65**, 27 (2002).
[4] J. Y. Marzin, J. M. Gerard, A. Izrael, D. Barrier, and G. Bastard, Phys. Rev. Lett. **73**, 716 (1994).
[5] A. D. Yoffe, Adv. Phys. **50**, 1 (2001).
[6] D. Bimberg, J. Phys. D **38**, 2055 (2005).
[7] F. Heinrichsdorff, M. H. Mao, N. Kirstaedter, A. Krost, D. Bimberg, A. O. Kosogov, and P. Werner, Appl. Phys. Lett. **71**, 22 (1997).
[8] A. D. Stiff, S. Krishna, P. Bhattacharya, and S. W. Kennerly, IEEE J. Quantum Electron. **37**, 1412 (2001).
[9] D. Loss and D. P. DiVincenzo, Phys. Rev. A **57**, 120 (1998).
[10] J. I. Martín, J. Nogués, K. Liu, J. L. Vicent, and I. K. Schuller, J. Magn. Magn. Mater. **256**, 449 (2003).
[11] J. G. Amar and F. Family, Phys. Rev. B **54**, 14742 (1996).
[12] K. Robbie and M. J. Brett, J. Vac. Sci. Technol. A **15**, 1460 (1997).
[13] S. van Dijken, L. C. Jorritsma, and B. Poelsema, Phys. Rev. Lett.

82, 4038 (1999).
[14] K. A. Fichthorn and W. H. Weinberg, J. Chem. Phys. **95**, 1090 (1991).
[15] F. Buatier de Mongeot, W. Zhu, A. Molle, R. Buzio, C. Boragno, U. Valbusa, E. G. Wang, and Z. Y. Zhang, Phys. Rev. Lett. **91**, 016102 (2003).
[16] W. Zhu, F. B. de Mongeot, U. Valbusa, E. G. Wang, and Z. Zhang, Phys. Rev. Lett. **92**, 106102 (2004).
[17] G. H. Vineyard, J. Phys. Chem. Solids **3**, 121 (1957).
[18] C. L. Liu, J. M. Cohen, J. B. Adams, and A. F. Voter, Surf. Sci. **253**, 334 (1991).
[19] G. Kresse and J. Hafner, Phys. Rev. B **47**, 558 (1993).
[20] G. Kresse and J. Furthmüller, Comput. Mater. Sci. **6**, 15 (1996).
[21] G. Kresse and J. Furthmüller, Phys. Rev. B **54**, 11169 (1996).
[22] G. Henkelman, B. P. Uberuaga, and H. Jónsson, J. Chem. Phys. **113**, 9901 (2000).
[23] D. Vanderbilt, Phys. Rev. B **41**, 7892 (1990).
[24] G. Kresse and J. Hafner, J. Phys.: Condens. Matter **6**, 8245 (1994).
[25] J. P. Perdew and Y. Wang, Phys. Rev. B **45**, 13244 (1992).
[26] N. D. Mermin, Phys. Rev. **137**, A1441 (1965).
[27] H. J. Monkhorst and J. D. Pack, Phys. Rev. B **13**, 5188 (1976).
[28] *AIP Handbook*, 3rd ed., edited by D. E. Gray (McGraw-Hill, New York, 1972).
[29] J. P. Perdew, K. Burke, and M. Ernzerhof, Phys. Rev. Lett. **77**, 3865 (1996).
[30] R. Stumpf and M. Scheffler, Phys. Rev. B **53**, 4958 (1996).
[31] Y. Tiwary and K. A. Fichthorn, Phys. Rev. B **75**, 235451 (2007).
[32] Y. Tiwary and K. A. Fichthorn, Phys. Rev. B **78**, 205418 (2008).
[33] H. B. Nielsen and D. L. Adams, J. Phys. C **15**, 615 (1982).
[34] J. Burchhardt, M. M. Nielsen, D. L. Adams, E. Lundgren, and J. N. Andersen, Phys. Rev. B **50**, 4718 (1994).
[35] F. Jona, D. Sondericker, and P. M. Marcus, J. Phys. C **13**, L155 (1980).
[36] J. R. Noonan and H. L. Davis, J. Vac. Sci. Technol. A **8**, 2671 (1990).
[37] J. Furthmüller, G. Kresse, J. Hafner, R. Stumpf, and M. Scheffler, Phys. Rev. Lett. **74**, 5084 (1995).
[38] J. Schöchlin, K. P. Bohnen, and K. M. Ho, Surf. Sci. **324**, 113 (1995).
[39] A. Kiejna and B. I. Lundqvist, Phys. Rev. B **63**, 085405 (2001).
[40] Y. Yourdshahyan, B. Razaznejad, and B. I. Lundqvist, Phys. Rev. B **65**, 075416 (2002).
[41] J. L. F. Da Silva, Phys. Rev. B **71**, 195416 (2005).
[42] G. Q. Huang, Phys. Rev. B **78**, 214514 (2008).
[43] B. W. Busch and T. Gustafsson, Surf. Sci. **415**, L1074 (1998).
[44] A. Mikkelsen, J. Jiruse, and D. L. Adams, Phys. Rev. B **60**, 7796 (1999).
[45] J. H. Petersen, A. Mikkelsen, M. M. Nielsen, and D. L. Adams, Phys. Rev. B **60**, 5963 (1999).
[46] H. Jónsson, G. Mills, and K. W. Jacobsen, in *Classical and Quantum Dynamics in Condensed Phase Simulations*, edited by B. J. Berne, G. Ciccotti, and D. F. Coker (World Scientific, Singapore, 1998), p. 385.
[47] P. A. Gravil and S. Holloway, Surf. Sci. **310**, 267 (1994).
[48] Sun Yu-Jie and Li Jia-Ming, Chin. Phys. Lett. **20**, 269 (2003).
[49] N. G. V. Kampen, *Stochastic Processes in Physics and Chemistry*, 3rd ed. (Elsevier, Amsterdam, 2007).
[50] K. A. Fichthorn, R. A. Miron, Y. Wang, and Y. Tiwary, J. Phys.: Condens. Matter **21**, 084212 (2009).
[51] R. Tung, Ph. D. thesis, University of Pennsylvania, 1980.
[52] R. T. Tung and W. R. Graham, Surf. Sci. **97**, 73 (1980).
[53] C. L. Chen and T. T. Tsong, Phys. Rev. Lett. **66**, 1610 (1991).
[54] G. L. Kellogg, *Microbeam Analysis—1986*, edited by A. D. Romig and W. F. Chambers (San Francisco Press, San Francisco, 1986), p. 399.
[55] P. Stoltze, J. Phys.: Condens. Matter **6**, 9495 (1994).
[56] L. Hansen, P. Stoltze, K. W. Jacobsen, and J. K. Norskov, Phys. Rev. B **44**, 6523 (1991).
[57] F. Montalenti and R. Ferrando, Phys. Rev. B **58**, 3617 (1998).
[58] S. Durukanoğlu, O. S. Trushin, and T. S. Rahman, Phys. Rev. B **73**, 125426 (2006).
[59] C. Mottet, R. Ferrando, F. Hontinfinde, and A. C. Levi, Surf. Sci. **417**, 220 (1998).
[60] C. M. Chang, C. M. Wei, and S. P. Chen, Phys. Rev. B **54**, 17083 (1996).
[61] M. Karimi, G. Vidali, and I. Dalins, Phys. Rev. B **48**, 8986 (1993).
[62] R. Sathiyanarayanan and T. L. Einstein, Surf. Sci. **603**, 2387 (2009).
[63] P. J. Feibelman, Phys. Rev. Lett. **65**, 729 (1990).
[64] P. J. Feibelman, Surf. Sci. **423**, 169 (1999).
[65] T. Fordell, P. Salo, and M. Alatalo, Phys. Rev. B **65**, 233408 (2002).
[66] A. Bogicevic, J. Strömquist, and B. I. Lundqvist, Phys. Rev. Lett. **81**, 637 (1998).
[67] J. V. Barth, H. Brune, B. Fischer, J. Weckesser, and K. Kern, Phys. Rev. Lett. **84**, 1732 (2000).
[68] G. Ehrlich and F. G. Hudda, J. Chem. Phys. **44**, 1039 (1966).
[69] R. L. Schwoebel and E. J. Shipsey, J. Appl. Phys. **37**, 3682 (1966).
[70] P. J. Feibelman, Phys. Rev. Lett. **81**, 168 (1998).
[71] A. Gölzhäuser and G. Ehrlich, Phys. Rev. Lett. **77**, 1334 (1996).
[72] T. Y. Fu, H. T. Wu, and T. T. Tsong, Phys. Rev. B **58**, 2340 (1998).
[73] O. V. Lysenko, V. S. Stepanyuk, W. Hergert, and J. Kirschner, Phys. Rev. Lett. **89**, 126102 (2002).
[74] A. S. Smirnov, N. N. Negulyaev, L. Niebergall, W. Hergert, A. M. Saletsky, and V. S. Stepanyuk, Phys. Rev. B **78**, 041405(R) (2008).
[75] S. J. Liu, H. C. Huang, and C. H. Woo, Appl. Phys. Lett. **80**, 3295 (2002).
[76] M. G. Lagally and Z. Y. Zhang, Nature (London) **417**, 907 (2002).
[77] J. Wang, H. C. Huang, and T. S. Cale, Modell. Simul. Mater. Sci. Eng. **12**, 1209 (2004).
[78] R. Ferrando, F. Hontinfinde, and A. C. Levi, Phys. Rev. B **56**, R4406 (1997).
[79] A. Videcoq, F. Hontinfinde, and R. Ferrando, Surf. Sci. **515**, 575 (2002).
[80] C. Ratsch, A. Zangwill, P. Šmilauer, and D. D. Vvedensky, Phys. Rev. Lett. **72**, 3194 (1994).
[81] K. A. Fichthorn and M. Scheffler, Phys. Rev. Lett. **84**, 5371 (2000).
[82] H. L. Yang, Q. Sun, Z. Y. Zhang, and Y. Jia, Phys. Rev. B **76**, 115417 (2007).